IAI Journals.ASM.org

Failure To Recruit Anti-Inflammatory CD103$^+$ Dendritic Cells and a Diminished CD4$^+$ Foxp3$^+$ Regulatory T Cell Pool in Mice That Display Excessive Lung Inflammation and Increased Susceptibility to *Mycobacterium tuberculosis*

Chaniya Leepiyasakulchai,[a] Lech Ignatowicz,[a] Andrzej Pawlowski,[b] Gunilla Källenius,[b] and Markus Sköld[a]

Department of Microbiology, Tumor and Cell Biology, Karolinska Institutet, Stockholm, Sweden,[a] and Department of Clinical Science and Education, Karolinska Institutet, Stockholm, Sweden[b]

Susceptibility to *Mycobacterium tuberculosis* is characterized by excessive lung inflammation, tissue damage, and failure to control bacterial growth. To increase our understanding of mechanisms that may regulate the host immune response in the lungs, we characterized dendritic cells expressing CD103 (α_E integrin) (αE-DCs) and CD4$^+$ Foxp3$^+$ regulatory T (T_{reg}) cells during *M. tuberculosis* infection. In resistant C57BL/6 and BALB/c mice, the number of lung αE-DCs increased dramatically during *M. tuberculosis* infection. In contrast, highly susceptible DBA/2 mice failed to recruit αE-DCs even during chronic infection. Even though tumor necrosis factor alpha (TNF-α) is produced by multiple DCs and macrophage subsets and is required for control of bacterial growth, αE-DCs remained TNF-α negative. Instead, αE-DCs contained a high number of transforming growth factor beta-producing cells in infected mice. Further, we show that T_{reg} cells in C57BL/6 and DBA/2 mice induce gamma interferon during pulmonary tuberculosis. In contrast to resistant mice, the T_{reg} cell population was diminished in the lungs, but not in the draining pulmonary lymph nodes (PLN), of highly susceptible mice during chronic infection. T_{reg} cells have been reported to inhibit *M. tuberculosis*-specific T cell immunity, leading to increased bacterial growth. Still, despite the reduced number of lung T_{reg} cells in DBA/2 mice, the bacterial load in the lungs was increased compared to resistant animals. Our results show that αE-DCs and T_{reg} cells that may regulate the host immune response are increased in *M. tuberculosis*-infected lungs of resistant mice but diminished in infected lungs of susceptible mice.

Mycobacterium tuberculosis, the causative agent of pulmonary tuberculosis (TB), remains a threat to global health and is a leading cause of death from infectious disease in the world (60). The murine model of pulmonary TB has demonstrated the critical role of proinflammatory effector functions mediated by activated macrophages (Mϕ) and major histocompatibility complex (MHC)-restricted T cell responses to control the infection and ameliorate disease (10, 42). Following *M. tuberculosis* aerosol infection, the differences in the ability to control bacterial growth, lung lesions, and survival between various inbred mouse strains are dramatic (2, 7, 27, 33, 44, 45, 59). It is interesting that *M. tuberculosis*-susceptible mice can display lesions similar to those in humans with active TB, including severe inflammation in infected lungs and extensive tissue damage (2, 27). Many of the observations made to explain susceptibility to *M. tuberculosis* infection using animal models have translated into human pulmonary TB, and susceptibility to mycobacterial infection is dramatically increased in, for example, immunocompromised patients (11, 19, 20, 34, 35, 41, 47). Still, the cause of naturally occurring susceptibility to *M. tuberculosis* in seemingly healthy individuals is poorly understood. Since the nature of the inflammatory response to *M. tuberculosis* in mice correlates with lung damage and inability to control the infection (reviewed in reference 7), we took advantage of wild-type (WT) mice that are either resistant (C57BL/6 and BALB/c) or susceptible (DBA/2) to *M. tuberculosis* infection (33, 44, 45). The mouse model allowed us to investigate immunoregulatory mechanisms in the lung tissue during pulmonary TB that may balance proinflammatory reactions and that control the infection and tolerogenic mechanisms induced to prevent tissue damage and loss of function.

The CD103 (integrin α_E) cell surface marker can be used to identify a unique CD11b$^-$ CD11c$^+$ CD103$^+$ dendritic cell (αE-DC) population located in the skin and at mucosal sites in the intestine and lungs (reviewed in reference 13). The role of lung αE-DCs in host immunity is not well characterized, especially during bacterial infections. Still, αE-DCs seem to have a distinct role in host immunity compared to proinflammatory CD103$^-$ DCs in the lung tissue (3, 30, 58). Lung αE-DCs have migratory properties and are able to take up antigens, including apoptotic cells, that are transported to draining lymph nodes (LN) and presented to MHC class I- or class II-restricted T cells (15, 16, 22, 46). Thus, αE-DCs in the lung mucosa are strategically located and likely to influence the host immune response during pulmonary TB.

In the present study, we show that *M. tuberculosis*-susceptible mice display worse lung lesions and reduced ability to control *M. tuberculosis* growth. We show that the number of lung αE-DCs

Received 22 June 2011 Returned for modification 28 July 2011
Accepted 19 December 2011
Published ahead of print 3 January 2012
Editor: J. L. Flynn
Address correspondence to Markus Sköld, markus.skold@ki.se.

doi:10.1128/IAI.05552-11

increases dramatically in *M. tuberculosis*-infected resistant mouse strains, while susceptible mice display a reduced number of αE-DCs, but not other myeloid cell subsets, in response to *M. tuberculosis* infection. During early and chronic stages of *M. tuberculosis* infection, lung αE-DCs have an anti-inflammatory cytokine profile compared to other monocyte, DC, Mϕ, and neutrophil subsets in the infected lungs. We also report that *M. tuberculosis* changes the functional potential of CD4$^+$ Foxp3$^+$ regulatory T (T_{reg}) cells, which induce gamma interferon (IFN-γ) 6 to 10 weeks postinfection (p.i.). The change in functional potential precedes a diminished pool of T_{reg} cells in the lungs, but not in the draining pulmonary lymph nodes (PLN), of susceptible mice at week 12 p.i.

MATERIALS AND METHODS

Mice. Female C57BL/6NCrl, BALB/cNCrl, and DBA/2NCrl mice (6 to 9 weeks old) were purchased from Charles River (Germany). The animals used in this study were housed under specific-pathogen-free conditions in a biosafety level 3 animal facility at the Astrid Fagraeus Laboratory, Swedish Institute for Communicable Disease Control. All animal experiments were conducted in accordance with the Swedish Animal Welfare Act and approved by the Swedish Institute for Communicable Disease Control and by the Stockholm North Ethical Committee, Swedish Board of Agriculture (permit numbers N343/7 and N369/10). The health status of the mice was monitored daily by animal care technicians or veterinarians to ensure humane treatment.

***M. tuberculosis* aerosol infection.** The clinical *M. tuberculosis* isolate, strain Harlingen, used for the *M. tuberculosis* aerosol infections was kindly provided by J. van Embden, National Institute of Public Health and the Environment, The Netherlands, and originally characterized by Kiers et al. (36). The bacteria were grown to mid-log phase in Sauton medium supplemented with 8 μg/ml polymyxin B and 5 μg/ml amphotericin B at 37°C, aliquoted, and stored in medium containing 10% glycerol at −80°C.

For aerosol infections, an *M. tuberculosis* aliquot was thawed at room temperature, spun at 10,000 rpm for 5 min, and triturated through a 25-gauge needle to disperse bacterial clumps. The bacterial suspension was diluted to 1×10^6 CFU/ml in sterile phosphate-buffered saline (PBS), 0.02% Tween 80, and placed in a nebulizer (MiniHeart Lo-Flo Nebulizer; Westmed, Tucson, AZ). The animals were infected with a low dose of *M. tuberculosis* via the respiratory route using a nose-only exposure system (In-Tox Products, Moriarty, NM) calibrated to deliver 20 to 200 CFU into the lungs. The animals were exposed to the *M. tuberculosis*-containing aerosol for 20 min. In some experiments, the number of viable bacteria that reached the lungs was determined on day 1 p.i. The aerosol infections were performed in the biosafety level 3 animal facility at the Astrid Fagraeus Laboratory, Swedish Institute for Communicable Disease Control.

CFU determination. The mice were anesthetized by exposure to isoflurane and euthanized by cervical dislocation. Both lungs were used for day 1 CFU determinations. For week 9 CFU determinations, only the right lung was used. For the later time point, blood was removed from the lung tissue by perfusing the heart with PBS, the tissue was aseptically removed, and the lungs were mechanically homogenized in PBS by passing the tissue through a steel mesh. Viable mycobacteria were quantified by plating the lung homogenates onto Middlebrook 7H11 agar plates. Colonies were counted after 2 to 3 weeks of incubation at 37°C.

Histology. Lung tissue from naïve or *M. tuberculosis*-infected mice was fixed in 4% paraformaldehyde and then embedded in paraffin. Five-micrometer tissue sections were stained with hematoxylin and eosin using a Shandon Varistain Gemini instrument or with Ziehl-Neelsen stain with the Putt modification to visualize acid-fast bacilli. Lung sections from 3 to 5 individual mice per group in two separate experiments were picked randomly and evaluated, blinded, for the relative size of the lung lesions, cellular infiltration, and the presence of acid-fast bacilli in infected mice.

***M. tuberculosis* cell wall extract.** The bacteria (H37Rv reference strain) were grown in Middlebrook medium at 37°C. The bacteria were centrifuged and heat killed at 70°C. The pellet was sonicated and freeze-dried on acetone with cotton.

Preparation of single-cell suspensions. At the indicated time points, single-cell suspensions were prepared from lungs and PLN. The mice were euthanized, and blood was removed from the lung tissue by perfusing the heart with PBS. The lungs and PLN were aseptically removed and placed in RPMI 1640 medium. The lungs were cut into small pieces and incubated in complete RPMI 1640 medium (supplemented with 10% fetal calf serum, penicillin-streptomycin, L-glutamine, sodium-pyruvate, and HEPES buffer, all from Sigma-Aldrich) containing 140 U/ml collagenase type IV (Sigma-Aldrich) for 90 min at 37°C, 5% CO_2. DNase I (Sigma-Aldrich) was added to the cell suspensions at a final concentration of 200 U/ml during the last 10 min of the incubation. The digested lung tissue was then passed through a steel mesh cup sieve (Sigma-Aldrich). Any remaining erythrocytes were lysed using lysis buffer (H_2O, 0.15 M NH_4Cl, 1 mM $KHCO_3$, 0.1 mM NaEDTA, pH 7.2 to 7.4), washed, and resuspended in RPMI 1640 medium. The cell suspension was passed through a 70-μm cell strainer (BD Falcon), washed, and resuspended in complete RPMI 1640 medium.

Single-cell suspensions were obtained from PLN using collagenase type IV and DNase I as described above. The PLN were then disaggregated using the frosted ends of two glass slides, washed, and resuspended in complete RPMI 1640 medium.

Total viable cells were enumerated using a hemocytometer and trypan blue exclusion of dead cells. Lung cells and PLN cells from infected mice were analyzed individually. PLN cells from naïve mice were pooled in each experiment.

Flow cytometry. Staining for surface markers was done by resuspending 2×10^6 cells in fluorescence-activated cell sorter (FACS) buffer (PBS with 1% [wt/vol] bovine serum albumin [BSA] and 2 mM NaN_3). The cells were incubated with purified anti-mouse CD16/CD32 (2.4G2; BD Pharmingen) at 20 μg/ml for 15 min at 4°C to block nonspecific binding. The cells were washed and incubated for 15 min at 4°C with primary antibodies specific for surface markers, or appropriate isotype controls, diluted in FACS buffer. The following allophycocyanin (APC)-, phycoerythrin (PE)-, PE-Cy7-, or peridinin chlorophyll protein (PerCP)-conjugated or biotinylated anti-mouse monoclonal antibodies (MAbs) were obtained from BD Pharmingen: anti-CD103 (M290), anti-CD11b (M1/70), anti-CD19 (1D3), anti-Ly6G (1A8), anti-Ly6C (AL-21), anti-CD3ε (145-2C11), and anti-CD4 (RM4-5). Streptavidin-Pacific orange was purchased from Invitrogen. The following fluorescein isothiocyanate (FITC)-, PE-, PE-Cy5.5-, APC-, Alexa Fluor 700-, or APC-Alexa Fluor 750-conjugated or biotinylated anti-mouse MAbs were purchased from eBioscience: anti-CD45.2 (104), anti-CD11c (N418), anti-CD11b (M1/70), anti-CD19 (1D3), anti-CD8α (53-6.7), anti-CD8β (H35-17.2), and anti-B220 (RA3-6B2). Anti-MHC class II (I-A/I-E)-PerCP (M5/114.15.2) was purchased from Biolegend. The stained cells were washed and fixed in freshly prepared 2% paraformaldehyde in PBS for 2 h at 4°C. Fixed cells were washed and resuspended in FACS buffer before analysis by flow cytometry.

For detection of inducible nitric oxide synthase (iNOS)-producing cells, the fixed cells were permeabilized for 20 min at room temperature using a Cytofix/Cytoperm kit from BD Biosciences. Intracellular iNOS was detected using an anti-iNOS-FITC MAb (clone 6; BD Transduction Laboratories) and compared to cells stained with a relevant isotype control MAb. The stained cells were washed and analyzed immediately by flow cytometry.

The cells were passed through a 70-μm nylon mesh before they were collected using a BD FACSAria (BD Biosciences) and analyzed using FlowJo software (version 8.8.6; Tree Star). All electronic gates and quadrants were set after relevant isotype control MAbs.

Foxp3$^+$ T_{reg} cells were identified at various time points after *M. tuberculosis* aerosol infection. After surface staining, the cells were washed,

fixed, permeabilized, and stained for intracellular Foxp3 by using an anti-mouse Foxp3-PE (MF23) MAb and mouse Foxp3 buffer set according to the manufacturer's instructions (BD Pharmingen).

***In vitro* stimulation of lung and PLN cells and intracellular-cytokine staining.** To examine the cytokine profile of myeloid cells, single-cell suspensions were prepared from *M. tuberculosis*-infected mice and kept in complete RPMI 1640 medium or stimulated with 100 ng/ml *Escherichia coli* lipopolysaccharide (LPS) (Sigma-Aldrich) or 10 μg/ml *M. tuberculosis* cell wall extract in the presence of 10 μg/ml brefeldin A (Sigma-Aldrich) for 5 h at 37°C, 5% CO_2.

Adherent cells were detached by incubating the cells in PBS, 2 mM EDTA, for 10 min at 37°C, 5% CO_2. The cells were stained for the indicated cell surface markers, fixed in 2% paraformaldehyde, permeabilized, and stained for intracellular cytokines: anti-tumor necrosis factor alpha (TNF-α)-FITC (MP6-XT22) (eBioscience) and anti-transforming growth factor beta (TGF-β)-APC (1D11) (R&D Systems) or relevant isotype controls. Stained cells were washed twice in permeabilization buffer and once with FACS buffer and analyzed immediately.

For determination of cytokine production by $CD4^+$ $Foxp3^-$ T cells and T_{reg} cells, single-cell suspensions from total lungs and PLN were kept in complete RPMI 1640 medium or stimulated with 50 ng/ml phorbol 12-myristate 13-acetate (PMA) (Sigma-Aldrich) and 10 μg/ml ionomycin (Sigma-Aldrich) in the presence of 10 μg/ml brefeldin A for 4 h at 37°C, 5% CO_2. The cells were then stained for the indicated lymphocyte surface markers, fixed using 2% paraformaldehyde, permeabilized, and stained for Foxp3 and IFN-γ (XMG1.2 conjugated to PE-Cy7; eBioscience) or relevant isotype controls.

RESULTS

Exacerbated lung lesions and higher bacterial burden in *M. tuberculosis*-infected lungs of susceptible mice. At mucosal surfaces, the immune system has to balance inflammatory reactions induced to eradicate potential harmful pathogens, such as *M. tuberculosis*, and at the same time avoid tissue damage and potential loss of function of the affected organ. During active pulmonary TB, the *M. tuberculosis*-induced lesions may erode the tissue as the disease progresses, leading to destruction of the lung architecture and scarring (12, 27).

We infected three groups of mice with a low dose (159 ± 46 CFU [mean ± standard deviation {SD}]; $n = 4$) of virulent *M. tuberculosis* (Harlingen strain) via the respiratory route and confirmed the striking differences in lung lesions and ability to control bacterial replication between resistant (C57BL/6 and BALB/c) and susceptible (DBA/2) inbred mice 9 weeks p.i. during chronic *M. tuberculosis* infection (Fig. 1) (33, 44). Hematoxylin and eosin staining showed that susceptible DBA/2 mice displayed larger lesions and more extensive loss of alveolar architecture (Fig. 1A) (4). Intracellular acid-fast bacilli were clearly detectable in infected lungs of all three mouse strains analyzed (Fig. 1B) (44). The ability to control bacterial replication 9 weeks p.i. was investigated by plating lung homogenates onto Middlebrook 7H11 agar plates (Fig. 1B). A significantly higher bacterial burden was observed in the lungs of BALB/c mice than in C57BL/6 mice (51). The bacterial burden in highly susceptible DBA/2 mice was approximately 10-fold higher in the lung tissue than in C57BL/6 and BALB/c mice (33, 44, 59).

By comparing WT inbred mouse strains that are either resistant or highly sensitive to low-dose virulent *M. tuberculosis* aerosol infection, we confirmed that susceptible mice have a more severe inflammatory reaction in the lungs and reduced ability to control bacterial growth (Fig. 1). Next, we asked how host immunity differs in animals that are resistant to *M. tuberculosis* infection compared to naturally susceptible WT mice. Therefore, we investigated the cellular infiltration in infected organs and the pro- and anti-inflammatory properties of the host immune response during pulmonary TB.

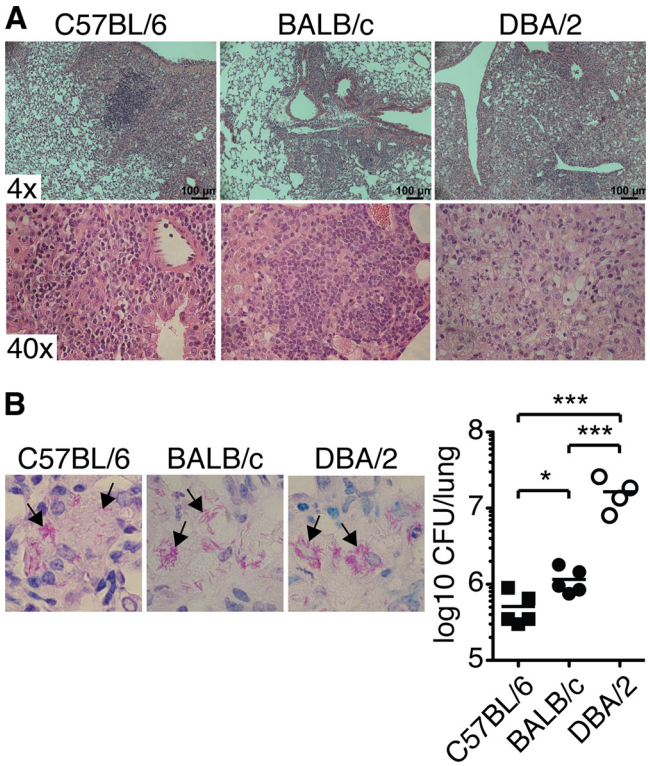

FIG 1 Lung lesions and bacterial burden in *M. tuberculosis*-infected mice. The photomicrographs show representative sections of formalin-fixed paraffin-embedded lung tissue stained with hematoxylin and eosin to determine lung pathology (A) or with Putt's stain to visualize acid-fast bacilli (B) from C57BL/6 (left), BALB/c (middle), and DBA/2 (right) mice infected with aerosolized virulent *M. tuberculosis* (9 weeks p.i.). (B, left) The arrows indicate examples of rod-shaped bacteria or clusters of bacteria. Magnification, ×100. (Right) CFU in the lungs 9 weeks p.i. Lung lesions and the ability to control *M. tuberculosis* growth were determined in two separate experiments, with 3 to 5 mice per group in each experiment. The graph shows means ± SEM from one representative experiment. *, $P < 0.05$; ***, $P < 0.001$ by one-way ANOVA with Bonferroni posttest.

Inflammatory monocyte recruitment into *M. tuberculosis*-infected lungs and Mϕ activation are not defective in susceptible mice. Using a monocyte adoptive-transfer model, we have directly shown that many of the Mϕ and DC subsets that appear in *M. tuberculosis*-infected lung tissue and draining PLN at the peak of the host immune response are monocyte derived (56). To determine if diminished monocyte recruitment may help explain naturally occurring susceptibility to *M. tuberculosis*, we examined the cellular infiltrate in resistant and susceptible lung tissue in uninfected mice and at various time points after virulent *M. tuberculosis* aerosol infection (Fig. 2). The CD11b/CD11c expression profile was determined on gated $CD45.2^+$ $CD19^-$ cells from naïve and *M. tuberculosis*-infected mice (Fig. 2A and data not shown). $CD11b^+$ $CD11c^-$ myeloid cells were then analyzed further. Recruited neutrophils were defined as $Ly6C^{int}$ (intermediate level of Ly6C) $Ly6G^+$ cells and inflammatory monocytes as $Ly6C^+$ $Ly6G^-$ cells (18, 56, 57). We found that the total number of lung cells increased dramatically in response to *M. tuberculosis* infection and

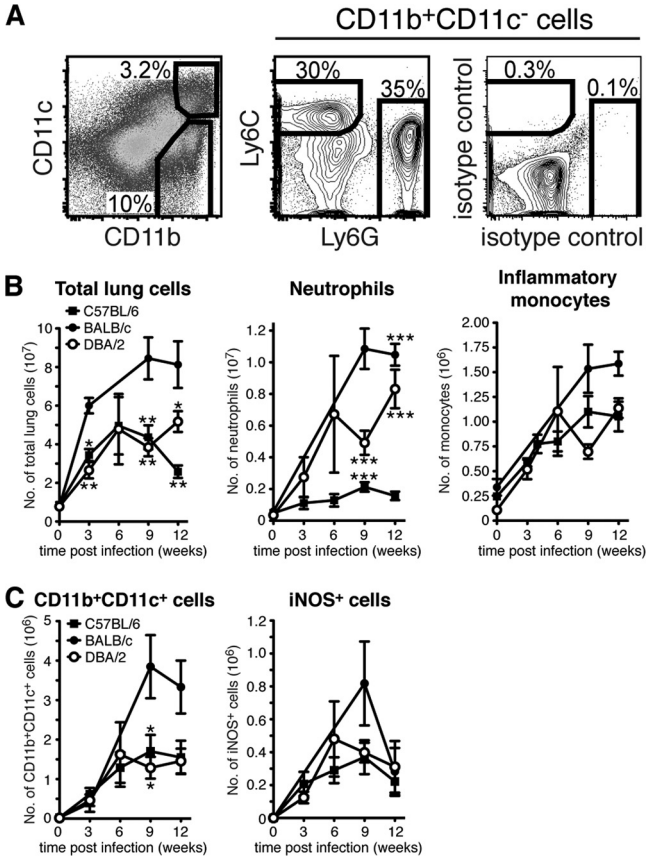

FIG 2 Neutrophil, inflammatory monocyte, DC, and Mϕ populations in the lungs of naïve and *M. tuberculosis*-infected mice. (A) Single-cell suspensions were prepared from the uninfected or *M. tuberculosis*-infected lung tissues of individual mice and stained for cell surface expression of CD11b and CD11c (left), Ly6G and Ly6C (middle), or isotype control MAbs (right). Ly6C$^+$ Ly6G$^-$ inflammatory monocytes and Ly6C^{int} Ly6G$^+$ neutrophils were identified within the CD11b$^+$ CD11c$^-$ gate (pregated on CD45.2$^+$ CD19$^-$ cells [data not shown]). The plots show lung cells analyzed 12 weeks p.i. from one representative experiment. (B) Graphs displaying the absolute numbers of total lung cells (left), neutrophils (middle), and inflammatory monocytes (right) in uninfected lungs and at various time points after *M. tuberculosis* infection. (C) Graphs displaying the absolute numbers of CD11b$^+$ CD11c$^+$ cells (left) in uninfected lungs and at various time points after *M. tuberculosis* infection. iNOS-producing cells were identified in the CD11b$^+$ CD11c$^+$ subset (right). The absolute number of myeloid cells was determined in 3 to 11 separate experiments with 2 or 3 mice per group in each experiment. The results were pooled from all replicate experiments. The graphs show means ± standard errors of the mean (SEM). Statistically significant differences between the mouse strains are denoted as follows: *, $P < 0.05$; **, $P < 0.01$; ***, $P < 0.001$ by one-way ANOVA with Bonferroni posttest.

was significantly higher in BALB/c mice than in C57BL/6 mice and DBA/2 mice at weeks 3, 9, and 12 p.i. (Fig. 2B) (33, 56). In the infected lung tissue of susceptible DBA/2 mice, the number of recruited neutrophils increased rapidly and continuously during the whole study period until 12 weeks p.i. (Fig. 2B). In comparison, neutrophil infiltration into the lung tissue of resistant C57BL/6 mice remained low. Still, levels of neutrophil recruitment into BALB/c and DBA/2 lungs were comparable, showing that neutrophil infiltration *per se* does not cause increased susceptibility to *M. tuberculosis* infection.

Following *M. tuberculosis* infection, Ly6C$^+$ inflammatory monocytes are recruited to the lung tissue (23, 56). Our results showed that there was no difference in the number of inflammatory monocytes recruited to *M. tuberculosis*-infected C57BL/6 and DBA/2 lungs (Fig. 2B). We also found that infected BALB/c lungs contained the highest number of recruited monocytes of the tested mouse strains 9 to 12 weeks p.i. (Fig. 2B). Our results suggest that defective monocyte recruitment into infected lungs does not explain increased susceptibility to *M. tuberculosis* in the mouse model.

Inflammatory monocytes recruited to the *M. tuberculosis*-infected lungs rapidly upregulate CD11c (56). The CD11b$^+$ CD11c$^+$ subset in inflamed or *M. tuberculosis*-infected lung tissue is a heterogeneous population, comprising both DCs and activated iNOS-producing Mϕ (23, 32, 39, 56). We enumerated CD11b$^+$ CD11c$^+$ myeloid cells in infected lung tissue to determine if susceptibility to *M. tuberculosis* can be explained by a reduced number of CD11b$^+$ CD11c$^+$ cells (Fig. 2C). In addition, because CD11b$^+$ CD11c$^+$ cells are the main producers of iNOS, an enzyme required for control of *M. tuberculosis* growth (42), we determined the number of activated iNOS-producing Mϕ in resistant and susceptible lungs (Fig. 2C). Upon *M. tuberculosis* aerosol infection of C57BL/6, BALB/c, and DBA/2 mice, the number of both CD11b$^+$ CD11c$^+$ cells and iNOS$^+$ Mϕ increased during the first 6 to 9 weeks p.i. before it reached a plateau and remained relatively constant, or even declined in BALB/c mice, until week 12 p.i. We did not detect a significant difference in the number of CD11b$^+$ CD11c$^+$ cells or iNOS$^+$ Mϕ between the three mouse strains tested. In conclusion, neither defective monocyte or neutrophil recruitment nor Mϕ activation seems to explain the increased susceptibility to *M. tuberculosis* in DBA/2 mice.

Diminished αE-DC population in the lungs of susceptible mice during pulmonary TB. αE-DCs have a distinct role in host immunity compared to proinflammatory CD103$^-$ lung DCs, including the cytokine and chemokine profile and the ability to migrate to the draining PLN for T helper cell activation or to cross-present antigens to MHC class I-restricted CD8$^+$ T cells (3, 14, 16, 46, 58). We characterized and enumerated lung αE-DCs to delineate their role in host immunity during pulmonary TB.

The αE-DC population in resistant and susceptible lung tissue was examined by flow cytometry in uninfected mice and at various time points after *M. tuberculosis* aerosol infection (Fig. 3). First, the CD11b/CD11c expression profile was determined on gated CD45.2$^+$ CD19$^-$ cells (Fig. 3A and data not shown). αE-DCs were identified in the CD11b$^-$ CD11c$^+$ myeloid cell subset in C57BL/6, BALB/c, and DBA/2 *M. tuberculosis*-infected lungs (Fig. 3A and data not shown). In all three mouse strains analyzed, αE-DCs expressed high levels of MHC class II and lacked expression of Ly6C, a marker for less differentiated cells, such as inflammatory monocytes, recruited to the *M. tuberculosis*-infected lung tissue (Fig. 3A) (56, 57).

Following *M. tuberculosis* infection, the number of αE-DCs increased early after infection (3 weeks p.i.) and remained high during chronic infection (weeks 9 to 12 p.i.) in resistant C57BL/6 and BALB/c mice (Fig. 3B). In comparison, accumulation of αE-DCs in susceptible mice was significantly reduced (Fig. 3B).

The increased number of αE-DCs in infected resistant mouse strains and the low numbers of αE-DCs in susceptible mice suggest that αE-DCs have a protective role in host immunity during pulmonary *M. tuberculosis*.

Susceptible mice display reduced numbers of αE-DCs in the draining PLN in response to *M. tuberculosis* infection. While

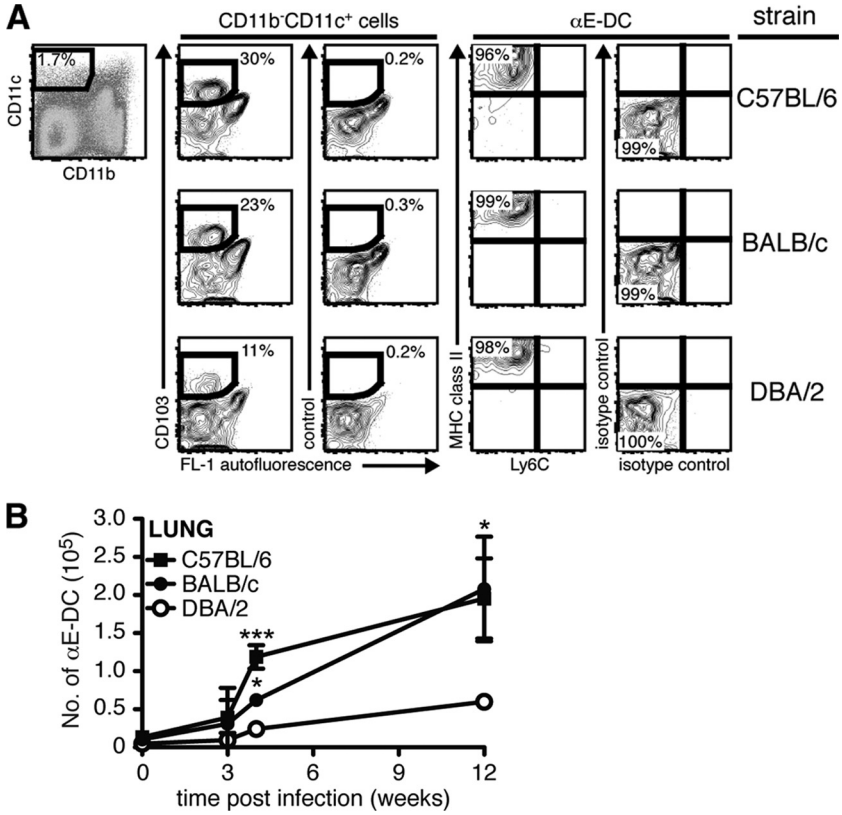

FIG 3 αE-DC populations in the lungs of naïve and *M. tuberculosis*-infected mice. (A) Groups of C57BL/6, BALB/c, and DBA/2 mice were infected with a low dose of virulent *M. tuberculosis* via the respiratory route. Single-cell suspensions were prepared from infected lungs 12 weeks p.i. and stained for CD45.2, CD19, CD11b, and CD11c (left and data not shown). αE-DCs were identified in the CD11b$^-$ CD11c$^+$ gate (pregated on CD45.2$^+$ CD19$^-$ cells [data not shown]) compared to an isotype control MAb (middle). The gated αE-DCs were examined for cell surface expression of Ly6C and MHC class II compared to isotype controls (right). The plots show lung cells from one representative experiment. (B) Graph showing the absolute numbers of αE-DCs in uninfected and *M. tuberculosis*-infected C57BL/6, BALB/c, and DBA/2 mice. Statistically significant differences between C57BL/6 and DBA/2 mice, or between BALB/c and DBA/2 mice, are indicated. At week 4 p.i., we also detected a statistically significant difference between C57BL/6 and BALB/c mice (**). The cell surface phenotype and the absolute number of αE-DCs were determined in nine separate experiments with 2 or 3 mice per group in each experiment. The results were pooled from all replicate experiments. The graphs show means ± SD. *, $P < 0.05$; **, $P < 0.01$; ***, $P < 0.001$ by one-way ANOVA with Bonferroni posttest.

alveolar Mϕ are considered to be the main target, DCs are infected by the bacterium and have been suggested to disseminate live *M. tuberculosis* via the lymphatics to the draining PLN, where the MHC-restricted T cell response is initiated (6, 61, 62). A more detailed analysis of the DCs that help spread *M. tuberculosis in vivo* is currently lacking. Considering the tissue localization of αE-DCs beneath the bronchial epithelial cell layer, their migratory potential and spreading of *M. tuberculosis* by infected DCs suggest that αE-DCs are involved in bacterial dissemination and priming of *M. tuberculosis*-specific CD8$^+$ T cells in the PLN (16, 46, 58, 62). Therefore, we determined if αE-DCs are present in the PLN of naïve mice after *M. tuberculosis* aerosol infection at the peak of the immune response and during chronic infection (Fig. 4). MHC class II^{hi} αE-DCs were identified in the CD11b$^-$ CD11c$^+$ gate in naïve C57BL/6 mice and in C57BL/6, BALB/c, and DBA/2 mice 3 weeks p.i. (Fig. 4A and B) (46). After *M. tuberculosis* infection, the total number of PLN cells seemed lower in DBA/2 mice, but due to the high variability between experiments, we did not detect a statistically significant difference (by one-way analysis of variance [ANOVA] with Bonferroni posttest) between the three mouse strains analyzed. Enumeration of PLN αE-DCs showed that the absolute number was significantly reduced in DBA/2 mice compared to C57BL/6 mice at both 3 and 9 weeks p.i. (Fig. 4C). The difference between C57BL/6 mice and BALB/c mice, and the difference between BALB/c mice and DBA/2 mice, was not statistically significant. Still, the trend was the same, with a higher number of αE-DCs in the more resistant BALB/c mice than in the DBA/2 mice. The reduced number of αE-DCs in the draining PLN may reflect reduced αE-DC migration from the *M. tuberculosis*-infected lungs in susceptible mice.

αE-DCs have a skewed cytokine profile during pulmonary TB. Sterile models of inflammation and *in vitro* studies have shown that αE-DCs are functionally different from other DC subsets found in the lung tissue, including the cytokine and chemokine profiles and different roles in T cell activation (3, 14, 16, 46, 58).

To determine the functional potential of αE-DCs and other myeloid cell subsets, including inflammatory monocytes, neutrophils, Mϕ, and DCs, we investigated the cytokine profiles during pulmonary TB (Fig. 5). Single-cell suspensions were prepared from total lung tissue of C57BL/6, BALB/c, and DBA/2 mice 3 or 12 weeks p.i. with a low dose of aerosolized *M. tuberculosis*. CD11b/CD11c profiling (gated on CD45.2$^+$ CD19$^-$ cells) (data not shown) was used to identify the main myeloid cell subsets in

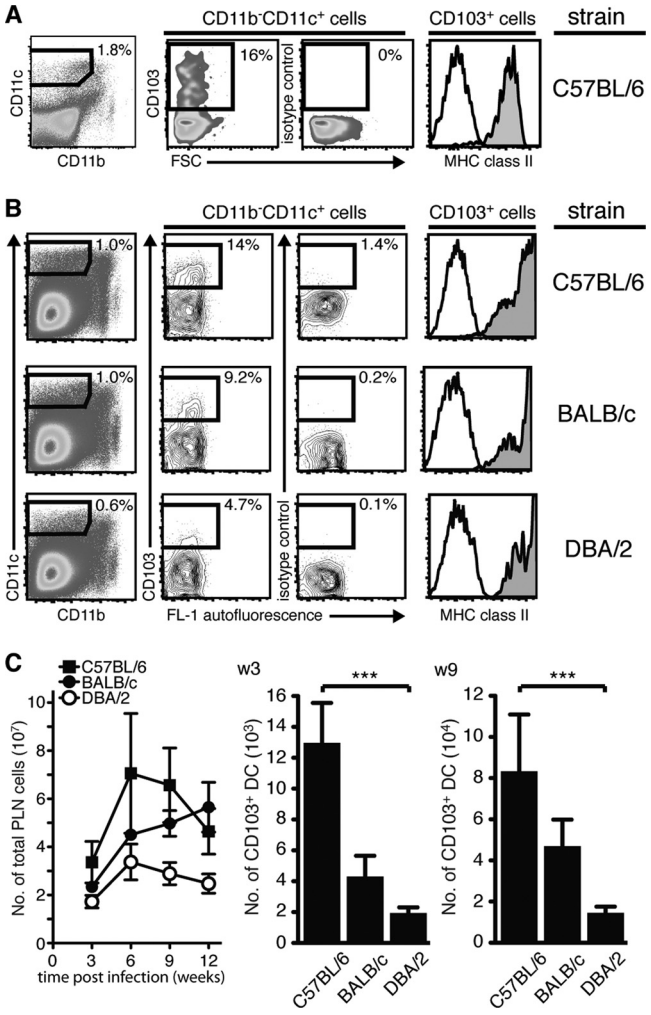

FIG 4 αE-DC populations in the PLN of naïve and *M. tuberculosis*-infected mice. (A) Single-cell suspensions were prepared from pooled PLN from five naïve C57BL/6 mice and stained for CD45.2, CD19, CD11b, and CD11c (left and data not shown) and for CD103 and MHC class II (right). αE-DCs were identified in the CD11b$^-$ CD11c$^+$ gate (pregated on CD45.2$^+$ CD19$^-$ cells [data not shown]) compared to an isotype control MAb. Gated αE-DCs were examined for cell surface expression of MHC class II (filled histograms) compared to an isotype control MAb (open histograms). (B) Groups of C57BL/6, BALB/c, and DBA/2 mice were infected with a low dose of virulent *M. tuberculosis* via the respiratory route. αE-DCs in the PLN were identified and analyzed as described for panel A. The plots show PLN cells analyzed 3 weeks p.i. from one representative experiment. (C) Graph showing the absolute number of PLN cells 3 to 12 weeks p.i. (left). The bar graphs show the absolute number of αE-DCs in *M. tuberculosis*-infected PLN 3 weeks (w3) or 9 weeks (9w) p.i. The cell surface phenotype and the absolute number of αE-DCs in the PLN were determined in three separate experiments with 2 or 3 mice per group in each experiment. The results were pooled from all replicate experiments. The graphs show means and SEM. ***, $P < 0.001$ by one-way ANOVA with Bonferroni posttest.

the infected lung tissue after *in vitro* stimulation (Fig. 5A). The percentage and absolute number of TNF-α- and TGF-β-producing cells, as well as the mean fluorescence intensity of the cytokine staining in positive cells, were compared in four myeloid cell subsets (Fig. 5A and B). The CD11b$^-$ CD11c$^+$ population was divided into αE-DCs and CD103$^-$ cells, which may contain alveolar Mϕ; CD11b$^+$ CD11c$^+$ cells (activated Mϕ and DCs); and CD11b$^+$ CD11c$^-$ cells (inflammatory monocytes and granulocytes) (23, 56).

TNF-α is a proinflammatory cytokine required for control of *M. tuberculosis* growth in both humans and mice (20, 35). In response to *M. tuberculosis* cell wall extract or LPS stimulation, several of the myeloid cell subsets (alveolar Mϕ, activated Mϕ and DCs, and inflammatory monocytes and granulocytes) contained a high proportion of TNF-α-producing cells. In contrast, in response to the same stimulation, αE-DCs remained essentially TNF-α negative (Fig. 5A and B). Here, we show that of all the myeloid cell subsets analyzed, αE-DCs in infected mice contained the highest percentage of TGF-β-producing cells (Fig. 5B). Interestingly, even though the absolute number of TGF-β-producing αE-DCs was clearly reduced in *M. tuberculosis*-susceptible DBA/2 mice, αE-DCs in *M. tuberculosis*-infected DBA/2 mice contained a significantly higher ($P < 0.01$ by one-way ANOVA with Bonferroni posttest) frequency of TGF-β-producing cells 3 weeks p.i.

To determine if the functional potential of αE-DC changes during the course of *M. tuberculosis* infection, we investigated the cytokine profile of αE-DCs in chronically infected mice (Fig. 5C). Similar to week 3 p.i., αE-DCs in C57BL/6, BALB/c, and DBA/2 mice remained TNF-α negative 12 weeks p.i. Also, even though the total number of TGF-β$^+$ αE-DCs was significantly reduced ($P < 0.001$ by one-way ANOVA with Bonferroni posttest) in DBA/2 mice, the αE-DC subsets in all three mouse strains tested contained similar high frequencies of TGF-β-producing cells in chronically infected mice. Accordingly, αE-DCs display an anti-inflammatory cytokine profile in *M. tuberculosis*-infected lungs compared to other myeloid cell subsets, a phenotype that was conserved between resistant and susceptible mouse strains and that was maintained during the course of the infection.

These results support an anti-inflammatory role for αE-DCs in host immunity during pulmonary TB.

Diminished Foxp3$^+$ T$_{reg}$ cell population in *M. tuberculosis*-infected lungs of susceptible mice. Excessive inflammatory reactions, including T cell activity, at mucosal surfaces can be detrimental to the host, resulting in tissue damage and loss of function of the affected organ. We determined if failure to recruit αE-DCs in *M. tuberculosis*-infected susceptible mice correlated with a reduced number of T$_{reg}$ cells in the infected lung tissue. Single-cell suspensions were prepared from *M. tuberculosis*-infected (3 or 12 weeks p.i.) C57BL/6, BALB/c, and DBA/2 lungs (Fig. 6A) and PLN (Fig. 6B). The cells were stained for cell surface expression of CD19, CD4, and CD8β (Fig. 6 and data not shown). After fixation, the cells were permeabilized and stained for intracellular expression of the transcription factor Foxp3. Foxp3 was not detected in CD8$^+$ T cells in the infected lungs or PLN (Fig. 6). Foxp3 expression is unique to T$_{reg}$ cells, and Foxp3 mRNA levels are the same in uninfected lungs of C57BL/6 and DBA/2 mice (21, 40). Also, we observed the same number of T$_{reg}$ cells in naïve C57BL/6 and DBA/2 lung tissue (data not shown). In agreement with previous findings, the CD4$^+$ T cell population in the lungs of C57BL/6 mice, and in BALB/c mice, contained a significant proportion of T$_{reg}$ cells that increased as the infection progressed (54). In contrast, the frequency of T$_{reg}$ cells was dramatically reduced in the CD4$^+$ T cell population early after *M. tuberculosis* infection at the peak of the immune response (3 weeks p.i.), and they were essentially absent from the chronically infected DBA/2 lungs (12 weeks p.i.).

Surprisingly, despite the difference in the CD4$^+$ T$_{reg}$ cell compartment in the *M. tuberculosis*-infected lungs of resistant and susceptible mice, no difference in the percentages or abso-

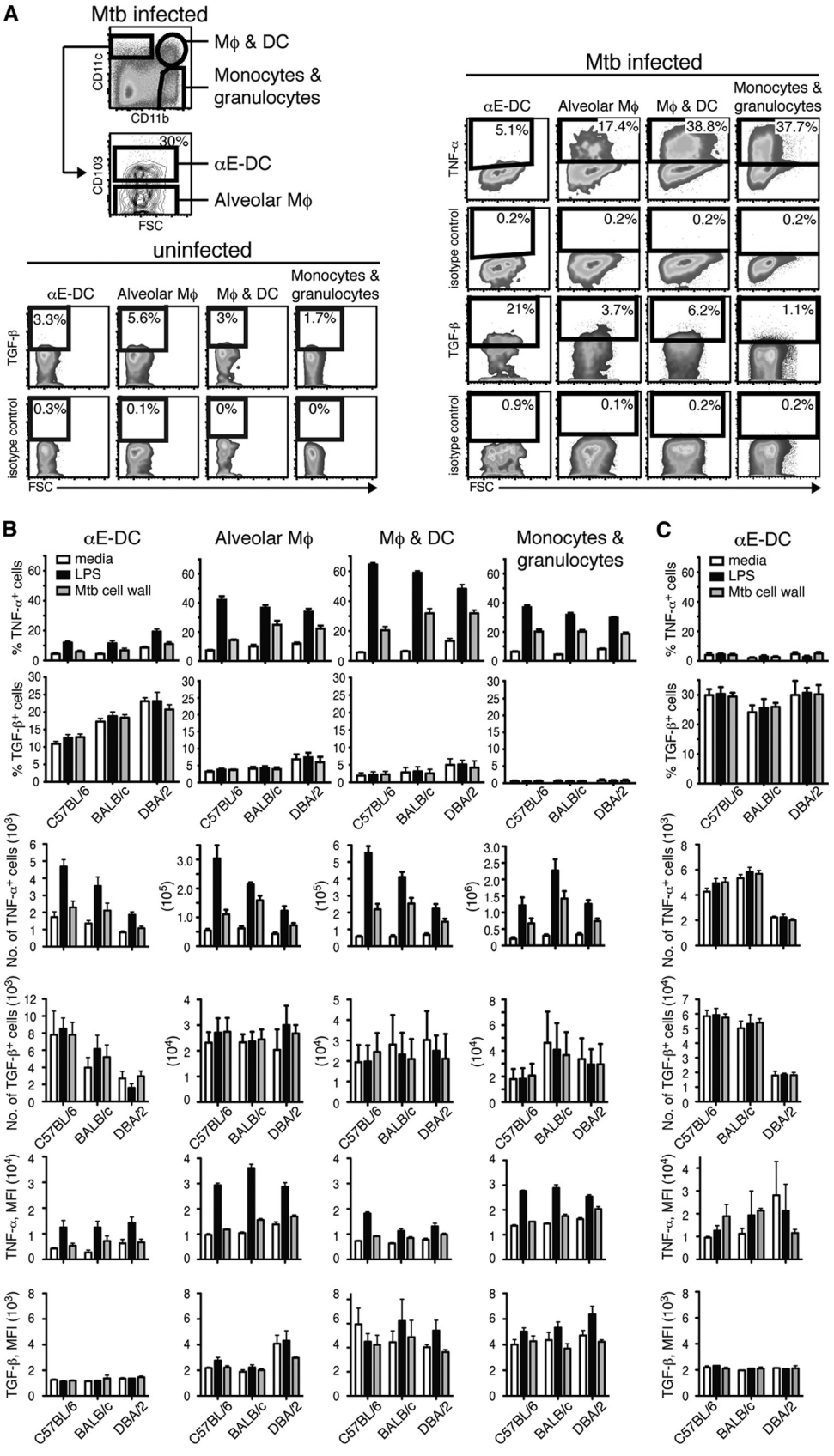
A
Mtb infected
Mϕ & DC
Monocytes & granulocytes
CD11c
CD11b
30%
αE-DC
Alveolar Mϕ
CD103
FSC
uninfected
αE-DC
Alveolar Mϕ
Mϕ & DC
Monocytes & granulocytes
TGF-β
isotype control
3.3%
5.6%
3%
1.7%
0.3%
0.1%
0%
0%
FSC
Mtb infected
αE-DC
Alveolar Mϕ
Mϕ & DC
Monocytes & granulocytes
TNF-α
isotype control
TGF-β
5.1%
17.4%
38.8%
37.7%
0.2%
0.2%
0.2%
0.2%
21%
3.7%
6.2%
1.1%
0.9%
0.1%
0.2%
0.2%
FSC
B
αE-DC
Alveolar Mϕ
Mϕ & DC
Monocytes & granulocytes
media
LPS
Mtb cell wall
% TNF-α+ cells
% TGF-β+ cells
No. of TNF-α+ cells (10³)
No. of TGF-β+ cells (10³)
TNF-α, MFI (10⁴)
TGF-β, MFI (10³)
C57BL/6
BALB/c
DBA/2
C
αE-DC
media
LPS
Mtb cell wall
% TNF-α+ cells
% TGF-β+ cells
No. of TNF-α+ cells (10³)
No. of TGF-β+ cells (10⁴)
TNF-α, MFI (10⁴)
TGF-β, MFI (10³)
C57BL/6
BALB/c
DBA/2

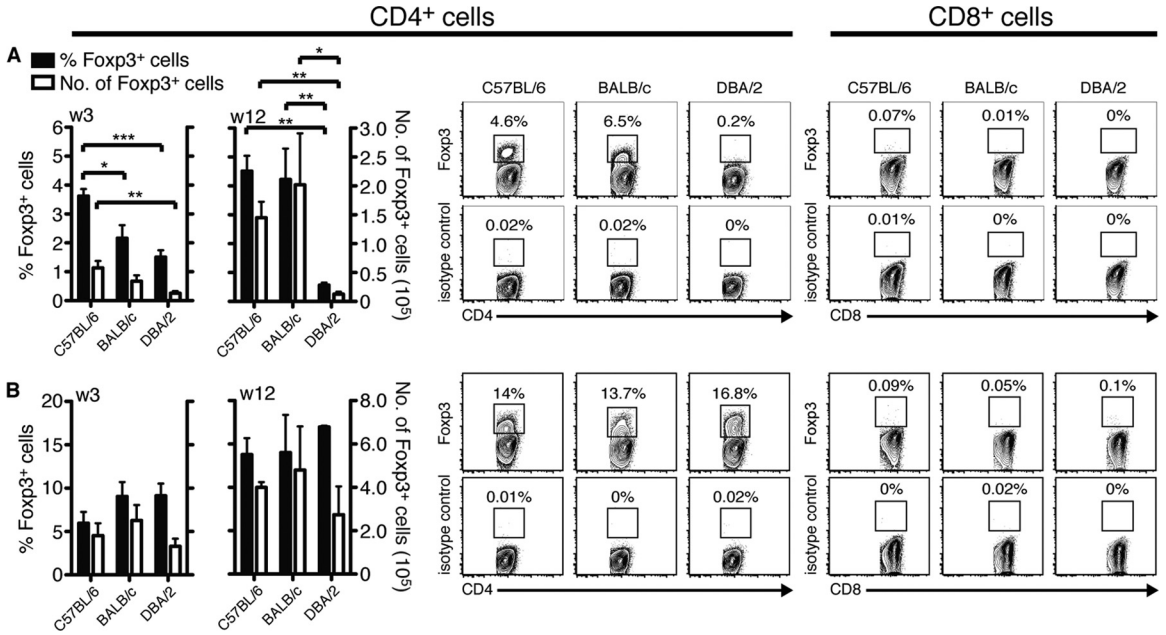

FIG 6 T_{reg} cell populations in the lungs and PLN of *M. tuberculosis*-infected mice. C57BL/6, BALB/c, and DBA/2 mice were infected with a low dose of aerosolized virulent *M. tuberculosis*, and the presence of T_{reg} cells in the infected lungs (A) and PLN (B) was analyzed three (w3), or 12 weeks (w12) p.i. The bar graphs show the percentages of T_{reg} cells among $CD4^+$ cells and the absolute numbers of T_{reg} cells in infected lungs (A) and PLN (B) of C57BL/6, BALB/c, and DBA/2 mice at the indicated time points after infection. The contour plots display Foxp3 expression in gated $CD4^+$ cells (left) and in gated $CD8^+$ cells (right) (week 12 p.i.; both T cell subsets were pregated on $CD19^-$ cells [data not shown]) compared to an isotype control. The $Foxp3^+$ T_{reg} population was analyzed in three separate experiments with five mice per group in each experiment. The plots show lung cells and PLN cells analyzed 12 weeks p.i. from one representative experiment. The results were pooled from all replicate experiments. The graphs display means and SEM. *, $P < 0.05$; **, $P < 0.01$; ***, $P < 0.001$ by one-way ANOVA with Bonferroni posttest.

lute numbers of $Foxp3^+$ T_{reg} cells was found in the draining PLN 3 or 12 weeks p.i. In all three mouse strains tested, the frequency and absolute numbers of PLN T_{reg} cells increased over time (Fig. 6B).

In summary, our results show that the reduced number of TGF-β-producing αE-DCs in *M. tuberculosis*-susceptible mice correlates with the diminished pool of $Foxp3^+$ T_{reg} cells during the peak of the immune response (week 3 p.i.) and in chronically infected lung tissue.

Increased IFN-γ production by T_{reg} cells in resistant and susceptible mice in response to *M. tuberculosis* infection. The absence of T_{reg} cells in chronically *M. tuberculosis*-infected susceptible lung tissue is reminiscent of the dramatically reduced number of T_{reg} cells found in the gut following lethal oral infection with *Toxoplasma gondii*, which is another T helper 1-inducing pathogen (48). The reduction in T_{reg} cell numbers in *T. gondii*-infected mice was accompanied by the induction of IFN-γ in the remaining T_{reg} cells (48). We therefore investigated if the functional potential of lung T_{reg} cells changed in response to *M. tuberculosis* infection (54). The data presented in Fig. 7 show that *M. tuberculosis* infection influenced the cytokine profile of T_{reg} cells in C57BL/6 and DBA/2 mice 6 to 10 weeks p.i. $CD4^+$ $Foxp3^-$ T cells and T_{reg} cells in naive and *M. tuberculosis*-infected lungs were stimulated polyclonally and analyzed for IFN-γ production. T cells from naïve mice kept in medium alone or stimulated with PMA and ionomycin contained few IFN-γ-producing cells (Fig. 7 and data not shown) (48). Similar to $CD4^+$ $Foxp3^-$ T cells, a large fraction of the stimulated T_{reg} cells in the lungs and PLN produced IFN-γ at 6 to 10 weeks p.i. We did not find any significant differences in the percentages of IFN-γ-producing $CD4^+$ $Foxp3^-$ T cells or T_{reg} cells between C57BL/6 and DBA/2 mice (Fig. 7B and C). After determining the absolute number of IFN-γ-producing T_{reg} cells in the lungs, we observed a statistically significantly higher number in C57BL/6 mice at weeks 6 and 10 p.i. (Fig. 7C). In the PLN, the absolute number of IFN-γ-producing T_{reg} cells was significantly higher in C57BL/6 mice only at week 6 p.i. Among $CD4^+$ $Foxp3^-$ T cells, we did not observe any significant differences in the PLN but did find a

FIG 5 αE-DC cytokine profile in *M. tuberculosis* (Mtb)-infected mice. Three mouse strains (C57BL/6, BALB/c, and DBA/2) were infected with a low dose of aerosolized virulent *M. tuberculosis*. Three or 12 weeks p.i., total lung cells were kept in medium or stimulated with LPS or *M. tuberculosis* cell wall extract. (A) The cell surface was stained for CD45.2 and CD19 (data not shown) and for CD11b, CD11c, and CD103 (top left). TNF-α and TGF-β production was compared between αE-DCs; $CD11b^-$ $CD11c^+$ $CD103^-$ cells, which may contain alveolar Mϕ; $CD11b^+$ $CD11c^+$ cells, which contain both activated Mϕ and DCs; and $CD11b^+$ $CD11c^-$ cells, which are monocytes and granulocytes right and bottom (left). The plots show *M. tuberculosis* cell wall extract-stimulated lung cells from uninfected mice or lung cells analyzed 3 weeks p.i. from one representative experiment. FSC, forward light scatter. (B) Bar graphs showing the percentages (top two rows), absolute numbers (middle two rows), and mean fluorescence intensity (MFI) (bottom two rows) of TNF-α- or TGF-β-producing αE-DCs in week 3 p.i. compared to the myeloid cell subsets shown in panel A. (C) Lung cells from C57BL/6, BALB/c, and DBA/2 mice were prepared 12 weeks p.i. as described above and analyzed for TNF-α and TGF-β production. The functional potential of αE-DCs was determined in four separate experiments with 2 or 3 mice per group in each experiment. The results were pooled from all replicate experiments. The graphs display means and SEM.

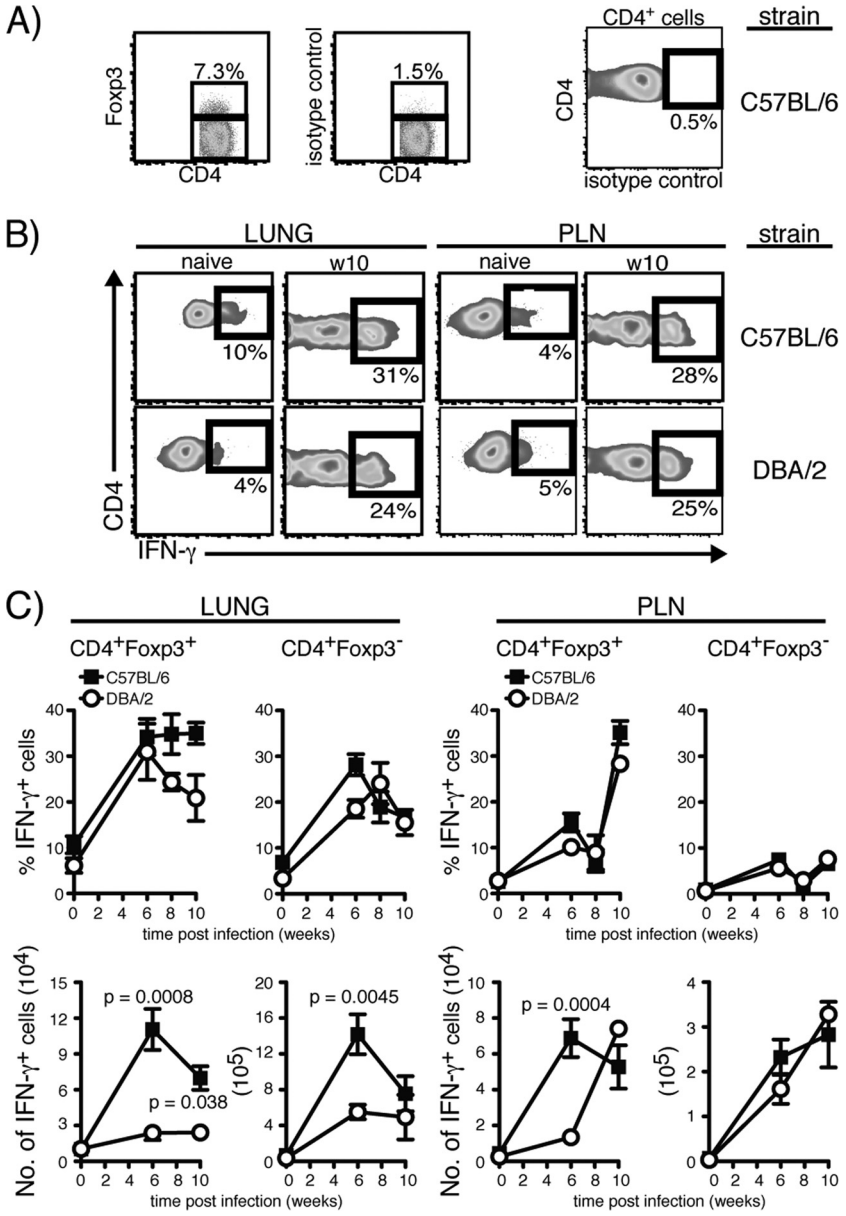

FIG 7 Cytokine production by T_{reg} cells during *M. tuberculosis* infection. Total lung cells and PLN cells were isolated from naïve or *M. tuberculosis*-infected C57BL/6 and DBA/2 mice and stimulated polyclonally *in vitro*. (A) Plots showing identification of lung $CD4^+$ $Foxp3^-$ T cells and T_{reg} cells (left) (pregated on $CD4^+$ $CD19^-$ cells [data not shown]). The gated cells were analyzed for intracellular cytokines using the gate set after the isotype control (right). The plots show stimulated lung cells analyzed 10 weeks p.i. from one representative experiment. (B) Plots showing stimulated lung T_{reg} cells (left) and PLN T_{reg} cells (right) from naïve mice or cells analyzed 10 weeks (w10) p.i. from one representative experiment. (C) Graphs showing the percentages (top) and absolute numbers (bottom) of IFN-γ-producing T_{reg} cells and $Foxp3^-$ $CD4^+$ T cells in uninfected and infected lung tissue (left) or in the PLN (right). The functional potential of T_{reg} cells was determined in two separate experiments with 2 or 3 mice per group in each experiment. The results were pooled from all replicate experiments. The graphs display means ± SEM, and a *t* test was used to determine statistical differences between C57BL/6 and DBA/2 mice at the various time points.

significantly higher number of IFN-γ producers in the lungs of C57BL/6 mice at week 6 p.i. (Fig. 7C).

In summary, our results show that T_{reg} cells in resistant and susceptible mice acquire the ability to produce IFN-γ in response to *M. tuberculosis* infection.

DISCUSSION

During pulmonary TB, disease progression in mice infected via the respiratory route is in many respects similar to human disease, including gradual progression of lung pathology, while other organs are less affected even though the bacteria can disseminate there from the lung tissue (2, 27). Animal models have proven useful in identifying factors important for control of mycobacterial growth, including proinflammatory mediators, like TNF-α or IFN-γ and the IFN-γ receptor (11, 19, 20, 34). Many of these findings have translated into human disease, and there are several studies demonstrating the importance of TNF-α, IFN-γ, and the IFN-γ receptor in the human immune response against mycobac-

terial infections, including *M. tuberculosis* (35, 41, 47). Still, susceptibility to *M. tuberculosis* in otherwise seemingly healthy individuals is poorly understood. In the present study, we took advantage of WT inbred mouse strains to increase our understanding of naturally occurring susceptibility to low-dose aerosol infection with virulent *M. tuberculosis*. Comparisons between different inbred WT mouse strains have identified numerous features of the host immune response that may help explain increased susceptibility to *M. tuberculosis* infection (2, 4, 6, 7, 27, 33, 44, 45, 59). For example, even though increased *M. tuberculosis* dissemination in the lung tissue has been shown to characterize susceptible mice (4), early *M. tuberculosis* dissemination from the lungs to the PLN may support a more robust *M. tuberculosis*-specific T cell response in resistant animals (6), and these T cells may localize more efficiently within the resistant lung tissue to help control the infection (59). The lungs pose a particular problem for the immune system trying to eradicate invading microorganisms, such as *M. tuberculosis*. While innate and adaptive immune effector functions are required for control of *M. tuberculosis* growth, excessive immune activation can lead to tissue damage and loss of function. Hence, a balance between inflammatory and tolerogenic immune reactions must be maintained at mucosal surfaces. This is illustrated by the extensive infiltration of lymphocytes and mononuclear cells into the lungs of Foxp3-deficient mice that lack T_{reg} cells (37). Here, we show that lung cells with anti-inflammatory effector functions are significantly reduced during chronic infection in *M. tuberculosis*-susceptible mice.

Recent studies using the mouse model have shown that T_{reg} cells are able to inhibit the antigen-specific T cell response during pulmonary TB and reduce the ability of the immune system to control bacterial growth (38, 54, 55). Also, in TB patients, the number of T_{reg} cells increases in infected tissues and isolated T_{reg} cells are able to suppress antigen-specific T cell responses *in vitro* (8, 24, 25, 53). However, the exact role of T_{reg} cells during pulmonary TB is not fully characterized. For example, while Scott-Browne reported that T_{reg} cell depletion reduces bacterial growth early after *M. tuberculosis* infection (54), Quinn et al. found that inhibition of T_{reg} cell activity *in vivo* prior to *M. tuberculosis* infection increased the frequency of IFN-γ- and IL-2-producing cells but had no effect on bacterial growth or lung lesions early after infection (52). Similarly, Ozeki et al. demonstrated that depletion of T_{reg} cells early after *M. tuberculosis* infection increased IFN-γ production by CD4$^+$ T cells and reduced the bacterial load. Interestingly, this effect was not observed if the T_{reg} cells were depleted at later stages of the infection, suggesting different roles for T_{reg} cells at early and later stages of pulmonary TB (50). Shafiani et al. used a different approach to investigate how T_{reg} cells influence *M. tuberculosis*-specific T cell immunity and bacterial growth early after *M. tuberculosis* infection (55). While the authors observed an increase in the lung CFU and a reduced number of *M. tuberculosis*-specific T cells in animals receiving adoptively transferred T_{reg} cells, the effects on the *M. tuberculosis*-specific T cell response was transient, and the effects on bacterial growth after day 35 p.i. were not determined (55). Our data show that *M. tuberculosis* infection induces IFN-γ production by T_{reg} cells by weeks 6 to 10 p.i. (Fig. 7). Even though we did not examine T_{reg} cell function at earlier time points, a possible explanation for the temporary effects observed by Shafiani et al. could be a change in the functional potential of the transferred cells in *M. tuberculosis*-infected recipients over time. The cytokine profile of T_{reg} cells in the lungs of *M. tuberculosis*-infected mice has been addressed by others (54). Scott-Browne et al. did not observe IFN-γ production by T_{reg} cells in response to *M. tuberculosis* infection. An explanation for the different findings may be found in how the cells were stimulated prior to intracellular-cytokine staining. We based our protocol on the work published by Oldenhove et al. and used PMA and ionomycin, while Scott-Browne et al. used anti-CD3 plus anti-CD28 stimulation (48, 54). Another explanation could be the use of different strains of *M. tuberculosis*, which can affect T cell function and lung pathology, depending on bacterial virulence (17, 49). We used the clinical *M. tuberculosis* isolate strain Harlingen, which, at least in *in vitro*-infected Mϕ, seems to be more virulent than the laboratory strain H37Rv used by Scott-Browne et al. and Carow et al. (5, 54).

M. tuberculosis-specific T cells are first detected in the PLN, but only after live bacteria have disseminated there from the lungs (6, 61). Even though the exact phenotype of the DCs that transport the bacteria to the PLN is not known, the majority of the infected cells in the PLN are CD11b$^+$ CD11c$^+$ at days 14 to 28 p.i. (62). Interestingly, *Mycobacterium bovis* BCG has also been suggested to disseminate in infected DCs (26). In the PLN, some of the BCG-infected DCs were reported to be CD11b negative, similar to αE-DCs (26). Since lung αE-DCs are migratory and are able to prime T cells in the PLN, perhaps *M. tuberculosis*-infected αE-DCs, or αE-DCs that have taken up infected cells undergoing apoptosis, are involved in initiating the adaptive T cell response during pulmonary TB (16).

Instead of observing an increased percentage of T_{reg} cells in infected susceptible lung tissue, which could help explain the increase in the bacterial burden, we found that the frequency of T_{reg} cells was significantly reduced 3 weeks p.i., and they were almost completely absent in chronically infected mice (Fig. 6). Thus, Foxp3$^+$ T_{reg} cell activity is less likely to explain the failure of the immune system in DBA/2 mice to control bacterial growth in the lungs at later stages of the infection. Despite the differences in the infected lungs, the frequency of Foxp3$^+$ T_{reg} cells in the CD4$^+$ T cell compartment in the PLN was not significantly different between the three mouse strains tested (Fig. 6). Therefore, the absence of T_{reg} cells in the chronically infected DBA/2 lungs was not due to systemic failure to generate T_{reg} cells in this susceptible mouse strain during chronic TB.

Why do T_{reg} cells not localize in the infected susceptible lungs? Because αE-DCs in the gut-associated lymphoid tissue are able to influence both priming and homing of MHC-restricted T cells and to induce T_{reg} cells to dampen overly aggressive immune responses (1, 9, 29, 31), we speculate that αE-DCs are analogues of their gut counterparts and play a role in host immunity during pulmonary TB by influencing T_{reg} cell biology in the lungs. αE-DCs have been shown to produce the chemokine CCL22 under steady-state conditions and during allergic airway inflammation (3). CCR4, the receptor for CCL22, is expressed on T_{reg} cells and induces T_{reg} cell migration (28). Moreover, a large fraction of lung αE-DCs are TGF-β^+ during TB (Fig. 5), and TGF-β is important for peripheral T_{reg} cell function and homeostasis (43). The reduced number of αE-DCs in *M. tuberculosis*-infected DBA/2 mice may therefore negatively affect T_{reg} recruitment or maintenance in the lungs.

αE-DCs have been shown to be Ly6C$^+$ monocyte derived under steady-state conditions (30). Our data show that monocyte recruitment is not defective in susceptible mice (Fig. 2B). Instead,

our results suggest that monocyte differentiation is altered in the *M. tuberculosis*-infected DBA/2 lung tissue. While the number of αE-DCs was reduced in infected susceptible mice, the number of $CD11b^+$ $CD11c^+$ cells and the number of iNOS-producing Mϕ were not (Fig. 2C) (33). In summary, changes in monocyte differentiation in *M. tuberculosis*-infected lung tissue likely explain the reduced number of αE-DCs in susceptible mice during pulmonary TB.

In conclusion, our results identify differences among αE-DCs and T_{reg} cells in *M. tuberculosis*-resistant and -susceptible inbred mice that may increase our understanding of immune regulation during pulmonary TB.

ACKNOWLEDGMENTS

This work was supported by grants from the Swedish Research Council (grant no. K2007-57X-20360-01-4), The Swedish Heart-Lung Foundation, Stiftelsen Clas Groschinskys Minnesfond, and Karolinska Institutet to M.S. C.L. was supported by a scholarship from the Royal Thai Government, and L.I. was the recipient of a Marie-Curie Host Fellowship for Early Stage Researchers Training grant and was supported by a grant from Stiftelsen Sigurd och Elsa Goljes Minne.

We acknowledge Markus Maeurer, Karolinska Institutet; Mats Spångberg and Helene Fredlund; and the staff of the biosafety level 3 animal facility, Astrid Fagraeus Laboratory, Swedish Institute for Communicable Disease Control, for their help in facilitating these experiments. We are grateful to Samuel Behar, Brigham and Women's Hospital and Harvard Medical School, for his help in establishing the aerosol infection model and for critically reading the manuscript and to Gunilla Högberg, Karolinska University Hospital, for her help with the lung histology.

REFERENCES

1. **Annacker O, et al.** 2005. Essential role for CD103 in the T cell-mediated regulation of experimental colitis. J. Exp. Med. **202**:1051–1061.
2. **Basaraba RJ.** 2008. Experimental tuberculosis: the role of comparative pathology in the discovery of improved tuberculosis treatment strategies. Tuberculosis **88**(Suppl. 1):S35–S47.
3. **Beaty SR, Rose CE Jr, Sung SS.** 2007. Diverse and potent chemokine production by lung CD11bhigh dendritic cells in homeostasis and in allergic lung inflammation. J. Immunol. **178**:1882–1895.
4. **Cardona PJ, et al.** 2003. Widespread bronchogenic dissemination makes DBA/2 mice more susceptible than C57BL/6 mice to experimental aerosol infection with Mycobacterium tuberculosis. Infect. Immun. **71**:5845–5854.
5. **Carow B, et al.** 2011. Silencing suppressor of cytokine signaling-1 (SOCS1) in macrophages improves Mycobacterium tuberculosis control in an interferon-gamma (IFN-gamma)-dependent manner. J. Biol. Chem. **286**:26873–26887.
6. **Chackerian AA, Alt JM, Perera TV, Dascher CC, Behar SM.** 2002. Dissemination of Mycobacterium tuberculosis is influenced by host factors and precedes the initiation of T-cell immunity. Infect. Immun. **70**:4501–4509.
7. **Chackerian AA, Behar SM.** 2003. Susceptibility to Mycobacterium tuberculosis: lessons from inbred strains of mice. Tuberculosis **83**:279–285.
8. **Chen X, et al.** 2007. CD4(+)CD25(+)FoxP3(+) regulatory T cells suppress Mycobacterium tuberculosis immunity in patients with active disease. Clin. Immunol. **123**:50–59.
9. **Coombes JL, et al.** 2007. A functionally specialized population of mucosal CD103+ DCs induces Foxp3+ regulatory T cells via a TGF-beta and retinoic acid-dependent mechanism. J. Exp. Med. **204**:1757–1764.
10. **Cooper AM.** 2009. Cell-mediated immune responses in tuberculosis. Annu. Rev. Immunol. **27**:393–422.
11. **Cooper AM, et al.** 1993. Disseminated tuberculosis in interferon gamma gene-disrupted mice. J. Exp. Med. **178**:2243–2247.
12. **Dannenberg Jr, AM.** 2006. Pathogenisis of human pulmonary tuberculosis: insights from the rabbit model. ASM Press, Washington, DC.
13. **del Rio ML, Bernhardt G, Rodriguez-Barbosa JI, Forster R.** 2010. Development and functional specialization of CD103+ dendritic cells. Immunol. Rev. **234**:268–281.
14. **del Rio ML, et al.** 2008. CX3CR1+ c-kit+ bone marrow cells give rise to CD103+ and CD103- dendritic cells with distinct functional properties. J. Immunol. **181**:6178–6188.
15. **del Rio ML, Rodriguez-Barbosa JI, Kremmer E, Forster R.** 2007. CD103- and CD103+ bronchial lymph node dendritic cells are specialized in presenting and cross-presenting innocuous antigen to CD4+ and CD8+ T cells. J. Immunol. **178**:6861–6866.
16. **Desch AN, et al.** 2011. CD103+ pulmonary dendritic cells preferentially acquire and present apoptotic cell-associated antigen. J. Exp. Med. **208**:1789–1797.
17. **Dunn PL, North RJ.** 1995. Virulence ranking of some Mycobacterium tuberculosis and Mycobacterium bovis strains according to their ability to multiply in the lungs, induce lung pathology, and cause mortality in mice. Infect. Immun. **63**:3428–3437.
18. **Fleming TJ, Fleming ML, Malek TR.** 1993. Selective expression of Ly-6G on myeloid lineage cells in mouse bone marrow. RB6-8C5 mAb to granulocyte-differentiation antigen (Gr-1) detects members of the Ly-6 family. J. Immunol. **151**:2399–2408.
19. **Flynn JL, et al.** 1993. An essential role for interferon gamma in resistance to Mycobacterium tuberculosis infection. J. Exp. Med. **178**:2249–2254.
20. **Flynn JL, et al.** 1995. Tumor necrosis factor-alpha is required in the protective immune response against Mycobacterium tuberculosis in mice. Immunity **2**:561–572.
21. **Fontenot JD, Gavin MA, Rudensky AY.** 2003. Foxp3 programs the development and function of CD4+CD25+ regulatory T cells. Nat. Immunol. **4**:330–336.
22. **GeurtsvanKessel CH, et al.** 2008. Clearance of influenza virus from the lung depends on migratory langerin+CD11b- but not plasmacytoid dendritic cells. J. Exp. Med. **205**:1621–1634.
23. **Gonzalez-Juarrero M, Shim TS, Kipnis A, Junqueira-Kipnis AP, Orme IM.** 2003. Dynamics of macrophage cell populations during murine pulmonary tuberculosis. J. Immunol. **171**:3128–3135.
24. **Guyot-Revol V, Innes JA, Hackforth S, Hinks T, Lalvani A.** 2006. Regulatory T cells are expanded in blood and disease sites in patients with tuberculosis. Am. J. Respir. Crit. Care Med. **173**:803–810.
25. **Hougardy JM, et al.** 2007. Regulatory T cells depress immune responses to protective antigens in active tuberculosis. Am. J. Respir. Crit. Care Med. **176**:409–416.
26. **Humphreys IR, et al.** 2006. A role for dendritic cells in the dissemination of mycobacterial infection. Microbes Infect. **8**:1339–1346.
27. **Hunter RL, Jagannath C, Actor JK.** 2007. Pathology of postprimary tuberculosis in humans and mice: contradiction of long-held beliefs. Tuberculosis **87**:267–278.
28. **Iellem A, et al.** 2001. Unique chemotactic response profile and specific expression of chemokine receptors CCR4 and CCR8 by CD4(+)CD25(+) regulatory T cells. J. Exp. Med. **194**:847–853.
29. **Jaensson E, et al.** 2008. Small intestinal CD103+ dendritic cells display unique functional properties that are conserved between mice and humans. J. Exp. Med. **205**:2139–2149.
30. **Jakubzick C, et al.** 2008. Blood monocyte subsets differentially give rise to CD103+ and CD103- pulmonary dendritic cell populations. J. Immunol. **180**:3019–3027.
31. **Johansson-Lindbom B, et al.** 2005. Functional specialization of gut CD103+ dendritic cells in the regulation of tissue-selective T cell homing. J. Exp. Med. **202**:1063–1073.
32. **Julia V, et al.** 2002. A restricted subset of dendritic cells captures airborne antigens and remains able to activate specific T cells long after antigen exposure. Immunity **16**:271–283.
33. **Jung YJ, Ryan L, LaCourse R, North RJ.** 2009. Differences in the ability to generate type 1 T helper cells need not determine differences in the ability to resist Mycobacterium tuberculosis infection among mouse strains. J. Infect. Dis. **199**:1790–1796.
34. **Kamijo R, et al.** 1993. Mice that lack the interferon-gamma receptor have profoundly altered responses to infection with Bacillus Calmette-Guerin and subsequent challenge with lipopolysaccharide. J. Exp. Med. **178**:1435–1440.
35. **Keane J, et al.** 2001. Tuberculosis associated with infliximab, a tumor necrosis factor alpha-neutralizing agent. N. Engl. J. Med. **345**:1098–1104.
36. **Kiers A, Drost AP, van Soolingen D, Veen J.** 1997. Use of DNA fingerprinting in international source case finding during a large outbreak of tuberculosis in The Netherlands. Int. J. Tuberc. Lung Dis. **1**:239–245.
37. **Kim JM, Rasmussen JP, Rudensky AY.** 2007. Regulatory T cells prevent

catastrophic autoimmunity throughout the lifespan of mice. Nat. Immunol. **8**:191–197.
38. **Kursar M, et al.** 2007. Cutting edge: regulatory T cells prevent efficient clearance of Mycobacterium tuberculosis. J. Immunol. **178**:2661–2665.
39. **Landsman L, Varol C, Jung S.** 2007. Distinct differentiation potential of blood monocyte subsets in the lung. J. Immunol. **178**:2000–2007.
40. **Lo Re S, et al.** 25 August 2011, posting date. PDGF-producing CD4+ Foxp3+ regulatory T lymphocytes promote lung fibrosis. Am. J. Respir. Crit. Care Med. doi:10.1164/rccm.201103-0516OC.
41. **Lopez-Maderuelo D, et al.** 2003. Interferon-gamma and interleukin-10 gene polymorphisms in pulmonary tuberculosis. Am. J. Respir. Crit. Care Med. **167**:970–975.
42. **MacMicking JD, et al.** 1997. Identification of nitric oxide synthase as a protective locus against tuberculosis. Proc. Natl. Acad. Sci. U. S. A. **94**: 5243–5248.
43. **Marie JC, Letterio JJ, Gavin M, Rudensky AY.** 2005. TGF-beta1 maintains suppressor function and Foxp3 expression in CD4+CD25+ regulatory T cells. J. Exp. Med. **201**:1061–1067.
44. **Medina E, North RJ.** 1996. Evidence inconsistent with a role for the Bcg gene (Nramp1) in resistance of mice to infection with virulent Mycobacterium tuberculosis. J. Exp. Med. **183**:1045–1051.
45. **Medina E, North RJ.** 1998. Resistance ranking of some common inbred mouse strains to Mycobacterium tuberculosis and relationship to major histocompatibility complex haplotype and Nramp1 genotype. Immunology **93**:270–274.
46. **Nakano H, et al.** 2012. Pulmonary CD103(+) dendritic cells prime Th2 responses to inhaled allergens. Mucosal Immunol. **5**:53–65.
47. **Newport MJ, et al.** 1996. A mutation in the interferon-gamma-receptor gene and susceptibility to mycobacterial infection. N. Engl. J. Med. **335**: 1941–1949.
48. **Oldenhove G, et al.** 2009. Decrease of Foxp3+ Treg cell number and acquisition of effector cell phenotype during lethal infection. Immunity **31**:772–786.
49. **Ordway D, et al.** 2007. The hypervirulent Mycobacterium tuberculosis strain HN878 induces a potent TH1 response followed by rapid down-regulation. J. Immunol. **179**:522–531.
50. **Ozeki Y, et al.** 2010. Transient role of CD4+CD25+ regulatory T cells in mycobacterial infection in mice. Int. Immunol. **22**:179–189.
51. **Paula MO, et al.** 2011. Host genetic background affects regulatory T-cell activity that influences the magnitude of cellular immune response against Mycobacterium tuberculosis. Immunol. Cell Biol. **89**:526–534.
52. **Quinn KM, et al.** 2006. Inactivation of CD4+ CD25+ regulatory T cells during early mycobacterial infection increases cytokine production but does not affect pathogen load. Immunol. Cell Biol. **84**:467–474.
53. **Ribeiro-Rodrigues R, et al.** 2006. A role for CD4+CD25+ T cells in regulation of the immune response during human tuberculosis. Clin. Exp. Immunol. **144**:25–34.
54. **Scott-Browne JP, et al.** 2007. Expansion and function of Foxp3-expressing T regulatory cells during tuberculosis. J. Exp. Med. **204**:2159–2169.
55. **Shafiani S, Tucker-Heard G, Kariyone A, Takatsu K, Urdahl KB.** 2010. Pathogen-specific regulatory T cells delay the arrival of effector T cells in the lung during early tuberculosis. J. Exp. Med. **207**:1409–1420.
56. **Skold M, Behar SM.** 2008. Tuberculosis triggers a tissue-dependent program of differentiation and acquisition of effector functions by circulating monocytes. J. Immunol. **181**:6349–6360.
57. **Sunderkotter C, et al.** 2004. Subpopulations of mouse blood monocytes differ in maturation stage and inflammatory response. J. Immunol. **172**: 4410–4417.
58. **Sung SS, et al.** 2006. A major lung CD103 (alphaE)-beta7 integrin-positive epithelial dendritic cell population expressing Langerin and tight junction proteins. J. Immunol. **176**:2161–2172.
59. **Turner J, et al.** 2001. Immunological basis for reactivation of tuberculosis in mice. Infect. Immun. **69**:3264–3270.
60. **WHO.** 2010. Global tuberculosis control: WHO report 2010. WHO/HTM/TB/2010.7. World Health Organization, Geneva, Switzerland.
61. **Wolf AJ, et al.** 2008. Initiation of the adaptive immune response to Mycobacterium tuberculosis depends on antigen production in the local lymph node, not the lungs. J. Exp. Med. **205**:105–115.
62. **Wolf AJ, et al.** 2007. Mycobacterium tuberculosis infects dendritic cells with high frequency and impairs their function in vivo. J. Immunol. **179**: 2509–2519.